

Expanding the Angle of Incidence Tolerance of Unclonable Anticounterfeiting Labels Based on Microlens Arrays and Luminescent Microparticles

Vinay Kumar, Stephan Dottermusch, Aditya Chauhan, Bryce S. Richards, and Ian A. Howard*

Unclonable anticounterfeiting labels can be based on micrometer-scale randomness created by stochastic processes like the distribution of luminescent microparticles in a transparent layer. Adding a microlens array to the layer can simplify the hardware needed for authentication in that magnification is no longer required. The bright point-pattern generated under light-emitting diode illumination can be captured by a standard digital camera. Shifting the angle of incidence (AOI) relocates the microlens foci changing the bright point-pattern. This provides unclonability, as several distinct bright point patterns at different AOI can be required for authentication. However, it also imposes technical requirements for the authentication setup in terms of the tolerance with which the AOI must be controlled. Herein, the AOI tolerance, the deviation of angle between reference and test image for which sufficiently similar bright point patterns are recorded that they are considered matching by the authentication algorithm, is investigated. Using microlens arrays with a focal length of $550\ \mu\text{m}$, the average size of the phosphor particle was varied from 9 ± 1 to $32.5 \pm 2\ \mu\text{m}$, resulting in a relaxation of tolerance from 0.8° to 3.6° . Methods to further increase the AOI tolerance and facilitate the practical implementation of these labels are discussed.

fake products in categories such as pharmaceuticals, electronics, and food.^[1] Counterfeiting is forecast to cost the global economy between 1.90 and 2.81 trillion USD and threaten 5.5 million jobs by 2022.^[2] There is continued interest in advancing anticounterfeiting technologies to mitigate the losses and risks caused by counterfeiting. The security of products against counterfeiting can be greatly enhanced by attaching a unique unclonable label to each product.^[3] For such an anti-counterfeiting system to be implemented, it must possess the following attributes: 1) the production of such a label should be straightforward but impossible to replicate; and 2) the authentication system should be economical and easy to implement. A brief overview of the state-of-the-art for some relevant unclonable anti-counterfeiting technologies employing optical authentication and their comparison is provided below.


Kumar et al. realized a lanthanide-based security ink consisting of $\text{Eu}^{3+}/\text{Tb}^{3+}/\text{Ce}^{3+}$ loaded Y_2O_3 nanorods dispersed in a poly-vinyl-chloride (PVC) medium. The ink was used to print a quick response (QR)-code that is unresponsive in the visible light but exhibits a strong multicolor-coded visible emission under UV illumination, which could be easily recognized by a smartphone.^[4] The unclonable nature of the labels was based on the random distribution of nanorods in a marked region of the QR-code, but to authenticate this a confocal microscope is necessary. Xie et al. developed a smart bi-layer system consisting of a polydimethylsiloxane (PDMS) substrate coated with anthracene and naphthalene diimide.^[5] Under the time-controlled exposure from a 365 nm ultraviolet (UV) source and a controlled thermal treatment of the masked substrate, a reversible dual-pattern of fluorescence emission and surface-wrinkled topography were observed by confocal microscopy. The random positioning of microwrinkled patterns on the PDMS substrate resulted from the manufacturing process.^[5] This dual-pattern not only functioned as an unclonable written message but also as a reusable substrate for secure data communication, as it was possible to erase the surface wrinkles by external stimuli, such as controlled thermal treatment,^[5] wavelength-selected light exposure,^[5] or via immersion in a

1. Introduction

Counterfeiting is a global issue that not only harms trade but also compromises human well-being through exposure to dangerous

V. Kumar, S. Dottermusch, A. Chauhan, B. S. Richards, I. A. Howard
Institute of Microstructure Technology
Karlsruhe Institute of Technology
Hermann-von-Helmholtz-Platz 1, 76344 Eggenstein-Leopoldshafen,
Germany
E-mail: ian.howard@kit.edu

B. S. Richards, I. A. Howard
Light Technology Institute
Karlsruhe Institute of Technology
Engesserstrasse 13, 76131 Karlsruhe, Germany

 The ORCID identification number(s) for the author(s) of this article can be found under <https://doi.org/10.1002/adpr.202100202>.

© 2022 The Authors. Advanced Photonics Research published by Wiley-VCH GmbH. This is an open access article under the terms of the Creative Commons Attribution License, which permits use, distribution and reproduction in any medium, provided the original work is properly cited.

DOI: 10.1002/adpr.202100202

pH-controlled solution.^[6] A metal-insulator-metal-based-plasmon enhanced upconversion (UC) luminescence label was developed by Park et al. in which a random network of Ag nanowires was deposited on a masked-UC-monolayer.^[7] The unique grid of crossing points of the Ag nanowires generated during the manufacturing provided an unclonable pattern.^[7] The formation of strong plasmonic hot spots at the crossing points of Ag nanowires led to enhancement of the UC luminescence of nearby nanophosphors, whose emission could then be captured with a standard digital camera. Recently, a smartphone-based authentication system was developed by Arppe-Tabbara and coworkers using a suspension of scattering microparticles sprayed on a printed QR-code.^[8] The randomly dispersed titania particles revealed a scattering pattern that was captured by a smartphone equipped with a macro lens for quick identification.^[8]

In our previous work, we implemented a microlens array (MLA) and an UC phosphor-doped PDMS matrix to develop an unclonable label.^[9] Upon illumination of the label with 980 nm laser light, a bright point-pattern of visible luminescence was generated. This point-pattern was caused due to much brighter emission from a microparticle phosphor when it lies in the focus of a microlens. Therefore, the point-pattern also changed when varying the angle of incidence (AOI), as the position of the focal volume for each microlens depends on the AOI. The unique and unclonable nature of the labels is due to the random alignment of the dispersed microparticles within the foci of the MLAs (see Section 1 of the Supporting Information, for a discussion on the randomness of the patterns created by these labels). However, the designed focal length (F) of the MLA ($F = 1900 \mu\text{m}$) together with the small-sized UC phosphor particles (around $10 \mu\text{m}$) meant that if the deviation of the AOI between the reference and test images was more than 0.2° then the test would not authenticate. This would mean that the positioning accuracy of the AOI achieved in field testing hardware must be 0.2° with respect to the AOI of the reference image such that they authenticate. Such a requirement for precise AOI control in the authentication equipment increases system complexity and limits the use-cases for this technology. In the current work, we extend our previous results by systematically examining how

the AOI tolerance (acceptable deviation in AOI between reference and test image) can be controlled and increased through label design. Expanding the tolerance for AOI mismatch between reference and test images is of practical interest as it reduces the requirement for the precision with which the angle between the label and the excitation source must be controlled and thereby decreases the complexity of the hardware needed for authentication.

2. Results

2.1. Label Design Principle

As outlined in our previous work, a bright point is created when the focal volume of a microlens (ML) coincides with a microparticle (see **Figure 1a**). Based on this arrangement, two variables are particularly important with regard to the AOI tolerance: 1) the focal length of the ML; and 2) the size of the microparticles (recall the AOI tolerance is the maximum deviation in AOI between the reference and test image for which the test image will still authenticate, see illustration in **Figure 1**). The focal length of the ML determines how far the focal volume shifts laterally for a given change in AOI. The mathematical expression of the lateral shift of foci, owing to a change of AOI ($d\theta$) is $\frac{dx}{d\theta} \approx F \sec^2\theta$, where F is the focal length of ML.^[9] For AOIs close to normal $\sec^2\theta \approx 1$ thus, simplifying to $dx \approx F d\theta$. In our previous work, we used an MLA with $F = 1900 \mu\text{m}$, leading to $dx \approx 38 \mu\text{m}/^\circ$. Previously, the focal length could not be shortened due to the thickness of the substrate used for the microlens layer ($1000 \mu\text{m}$). In comparison, we have adjusted the fabrication procedure to use a thinner substrate ($\approx 400 \mu\text{m}$, see the section below) that enables the use of a shorter focal length ($F = 550 \mu\text{m}$). This reduces dx by a factor of 3.4 to $\approx 10 \mu\text{m}/^\circ$ and should increase the tolerance of the bright point pattern to small changes in the AOI.

The AOI tolerance is also affected by the particle size, as the focal volume will remain within a particle longer when the particle is larger. To test the effect of particle size on the system's tolerance for angular positioning, commercially available

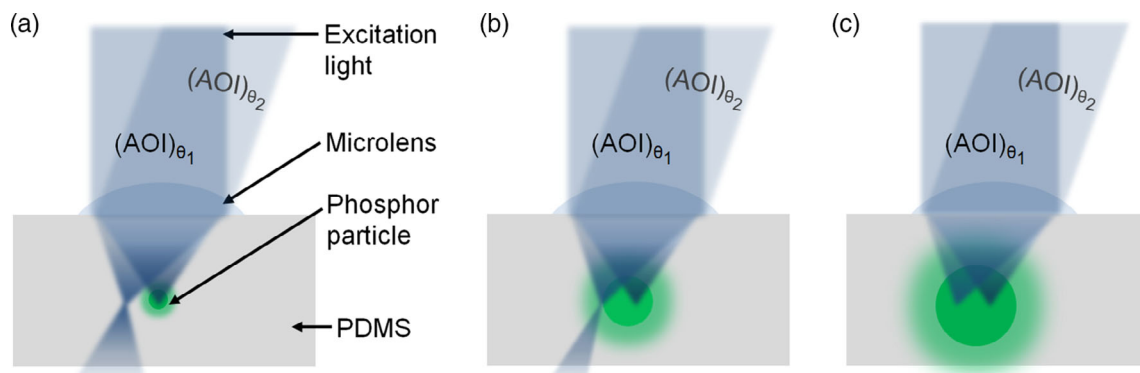


Figure 1. Schematic illustration of the effect of particle size on the tolerance of the bright point pattern against deviation of the angles of incidence (AOI). For smaller particles, a) a slight change in the AOI will cause the focal volume to move outside the particle volume and the bright point pattern will change. Thus precise control of AOI is needed for a test image to authenticate with a given reference image. As the particles become bigger; b,c), the bright point pattern should remain more similar for slightly differing AOIs, and the authentication tolerant to larger differences in AOI between the reference and test image.

downshifting (DS) phosphors of three different sizes were investigated: YYG-547-210, YYG-560-200, and YYG-557-230 isophor (Sigma-Aldrich) and possessed D50 particle size specified as 9.0 ± 1 , 20.5 ± 1 , and $32.5 \pm 2 \mu\text{m}$, respectively. The phosphor themselves are cerium-activated aluminum-garnet materials with an absorption band in the visible region (400–540 nm) and a broad emission window (470–700 nm). The scanning electron microscopy (SEM) images and measured optical spectra of the phosphors are provided in the Supplementary information (Supporting Information, Section 2 and 3). For simplicity, the designation S, M, and L have been used henceforth to refer the three phosphors with the small, medium, and large particle sizes. A schematic displaying the effects of an increase in particle size on the point-pattern generation in the three labels under different AOIs is presented in Figure 1. We hypothesize that the AOI tolerance will be proportional to particle size. Hence, by combining larger particles with shorter focal length lenses, we will be able to extend the AOI tolerance beyond the 0.2° demonstrated in our previous work.

2.2. Label Fabrication

The procedure for label fabrication is schematically depicted in Figure 2a. This is a slightly modified version of the previously reported method, which allows the lenses with a shorter focal

length to be used.^[9] First, a thin PDMS layer doped with the DS phosphor is deposited on a glass slide. The S, M, or L, phosphor particles are first mixed in the PDMS base (SYLGARD 184, DowSil, RTV-615, Component A) using a high-speed dispersion device (CAT M. zipper GmbH) such that the end concentration of the phosphors in the PDMS layer is 0.5 wt%. Then the particle-containing base is mixed with the curing agent (10:1 ratio, RTV-615, component-B) and deposited on the glass slide. Two strips of adhesive tape (Greenback tape 851, 3M) are attached to the slide and serve as spacers of 200 μm thickness. A glass coverslip with a thickness of 400 μm is then pressed down to laminate the PDMS between the slide and coverslip. The replication of the microlens features onto this thinner coverslip allows the decrease in focal length compared to our previous design.

Once the PDMS is cured, a microlens array is replicated onto the front side of the glass coverslip. Firstly, a MLA master structure is produced by two-photon lithography into IP-S photoresist (Nanoscribe) that was coated on an indium tin oxide (ITO)-coated glass slide. The lenses have a radius of curvature (ROC) of 200 μm and a base of 250 μm . The MLA array is a square lattice of 16×16 lenses with a center-to-center distance of 250 μm . This MLA master structure is then inversely replicated onto a PDMS stamp layer. Further, a UV-curable resin (Norland NOA-88 optical adhesive), is dropped onto the coverslip then imprinted with the PDMS. The sample is placed in a vacuum (0.2 Pa) for 10 min to remove bubbles. Thereafter, the bubble-free sample is UV

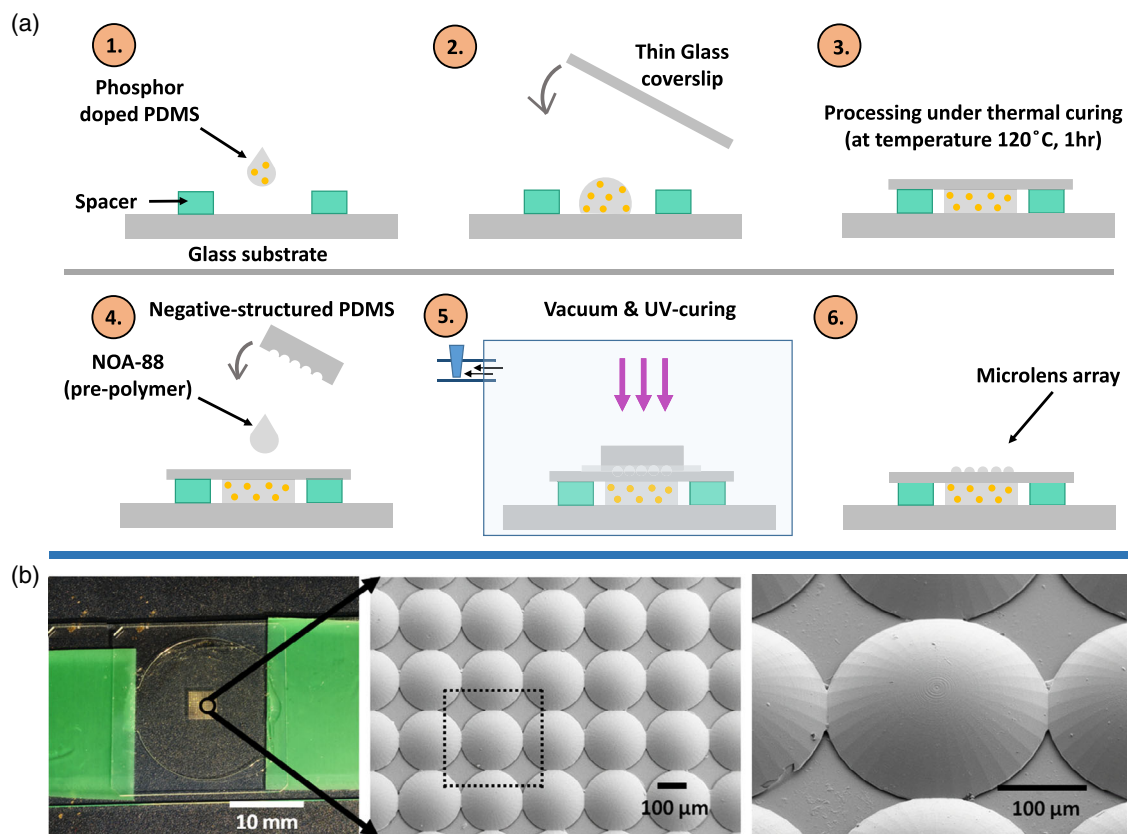


Figure 2. a) Schematic depicting the various steps involved in the fabrication process of the label. b) Optical photograph (top view) and the corresponding SEM images of the MLA attached to the label. Scale bar in the right-most panel holds true only along the measurement (horizontal) direction.

cured (365 nm, $\approx 10^3$ mW cm⁻²) for 2 min. Finally, the stamp is peeled away. Before each imprint, the PDMS stamp is processed with a vapor deposition of the antiadhesive layer (trichloro-1H,1H,2H,2H-perfluorooctyl-silane, Sigma-Aldrich), which assists the removal of the inverse PDMS stamp from the UV-cured MLA structures.

A photograph of the finished label is provided in Figure 2b. SEM images of the MLA replicated in the NOA-88 confirm the smooth and fine profile of the individual micro-lenses, which are arranged in a square close-packing pattern (Figure 2b). Complete details of the fabrication process are provided in the Material and Methods section. Given the index of refraction (n) of the cured NOA-88 as 1.57, the focal length of the 550 μ m is achieved using ($F = ROCn/(n - 1)$).

2.3. Qualitative Analysis: Angle of Incidence Tolerance and Particle Size

To qualitatively compare the similarity of the bright point patterns under different AOIs for labels prepared with S, M, and L particles, the following arrangement was used. A luminescence point-pattern was generated under the illumination of 450 nm LED (M450LP1, Thorlabs) at three different AOIs, which was captured by a scientific-CMOS camera (CS2100M, Thorlabs) equipped with a zoom lens (MVL7000, Thorlabs), facing the backside of the label. A 500 nm long-pass filter (FEL0500, Thorlabs) was used before the camera aperture to reject the light from the source. The three labels were placed on a motorized

rotation stage (CR1/M-Z7, Thorlabs) and the bright point-pattern images from each of the three labels were acquired at three different AOIs defined by rotating the label (0°, 2°, and 4°). **Figure 3** shows the acquired images of the luminescence point-patterns. The images are binarized by finding the noise level of the image in the region outside the MLA, then a value of “1” is assigned to pixels with a value greater than three times the noise level and zero to all remaining pixels. From the binary image, adjoining bright regions are ascertained and itemized. The details of image processing steps and the authentication algorithm is explained below in the Materials and Methods section under “pattern authentication algorithm.” For each label, the image at AOI = 0° is shown in red, at AOI = 2° in green, and at AOI = 4° in blue. Finally, a composite image is created by combining the images for all the three AOIs, and displayed in the last panel to compare the similarity of the point-patterns observed at the different AOIs. A combination of similarly positioned bright points in the AOI = 0° (red) and AOI = 2° (green) images will lead to yellow points, a combination of similarly position points in the AOI = 2° (green) and AOI = 4° (blue) images will lead to cyan points. Finally, a combination of similarly positioned points in the AOI = 0° (red), AOI = 2° (green), and AOI = 4° (blue) images will lead to white points. For the S label, the composite image has few white points, most points are either yellow (red + green) or cyan (green + blue), or red or blue alone. This suggests that most of the AOI = 2° (green) match with either and AOI = 0° (red) or an AOI = 4° (blue) point, but very few points are the same in all images. For the M image, the number of white points has increased and also many points are yellow

Particle Diameter (∅, D50)	Angle (θ, in deg)			Combined image Angles
	0°	2°	4°	
Label S (∅ = 8 – 10 μ m)				
Label M (∅ = 19.5 – 21.5 μ m)				
Label L (∅ = 30.5 – 34.5 μ m)				

Figure 3. Qualitative analysis of labels S, M, and L containing DS phosphors of different particle sizes. The binary images of the point-pattern at AOI = 0°, 2°, and 4° are shown in red, green, and blue, respectively. The final panel combines the three previous images into an RGB image. The overlapping bright points under all three AOIs appears as white dots, whereas the overlap of bright points from red and green lead to yellow dots, and from green and blue to cyan dots.

or cyan. This indicates an increased number of bright points that remain in the same position as compared with the S label. Finally, for the L label, even more of the points have become white, demonstrating that an even larger fraction of the bright points is in the same location irrespective of the AOI for these largest particles.

Thus, these raw qualitative results show that similar bright point patterns are measured over larger changes in AOI for larger particles as compared with the limited similarity range for smaller particles. For the largest particles, it appears that the bright point pattern is tolerant to a change in AOI of several degrees. We will now quantitatively investigate the probability for authentication as a function of the difference in AOIs between two images for the S, M, and L labels.

2.4. Quantitative Analysis: Angle of Incidence Tolerance and Particle Size

In our previous work, we established an algorithm to binarize the bright point patterns, then compare a test image to a reference image.^[9] The algorithm outputs a number of “votes” which represents the number of points it considers for matching between the two images. A threshold number of votes, above which the test and reference images are considered to be the same, can be determined by the analysis of a sufficiently large set of images with known reference and test pairs. These reference and test pairs are separated into two sets, consisting of pairs that should authenticate and those that should not. Previously, we performed such analysis on 10 000 image comparisons for four equivalent labels, with equivalent being understood as having the same processing conditions, but naturally different bright point-

patterns owing to the uniqueness of each label attributed to stochastic variation in microparticle positions.^[9] This led to a threshold number of 15 votes above which one could consider the test and reference as matching and therefore the label as authentic. As described in Section 4 of the Supporting Information, we perform a similar analysis for these new labels. For each of the new label design (S, M, and L), a comparison of 784 images revealed that the center of the histogram for the number of votes cast between the matching and nonmatching images are clearly separated. An average of almost 30 votes are cast when test and reference images should match, whereas the average number of votes is 5 if the test image should not match with the reference image. Hence, selecting a threshold of 16 votes will enable the authentication with good accuracy, similar to our previous label implementation.

To ascertain the AOI tolerance of the three labels, each label was placed on the sample stage, and images were captured from $\text{AOI} = 0^\circ$ to 20° at every 0.2° . The 41 images from $\text{AOI} 6^\circ$ to 14° were each considered as reference images (y -axis, Figure 4a). Each reference image was then compared with 61 adjacent images having an angular offset varying from -6° to $+6^\circ$ with respect to the AOI for reference image (x -axis, Figure 4a). The z -axis (color scale) shows the number of votes cast for the test images when compared with the reference images. For each label, 30 votes are cast (red color) under small angular offsets. However, after a certain angular offset with respect to the reference image, the number of cast vote drops rapidly. We recall that 16 (green color) or more votes must be cast for positive authentication. For each angular offset, the fraction of the 41 reference image AOIs that lead to more than 16 votes is tabulated. These values are presented for each label in Figure 4b and define the probability that a positive authentication will result for a given angular offset between the reference and test image. Further,

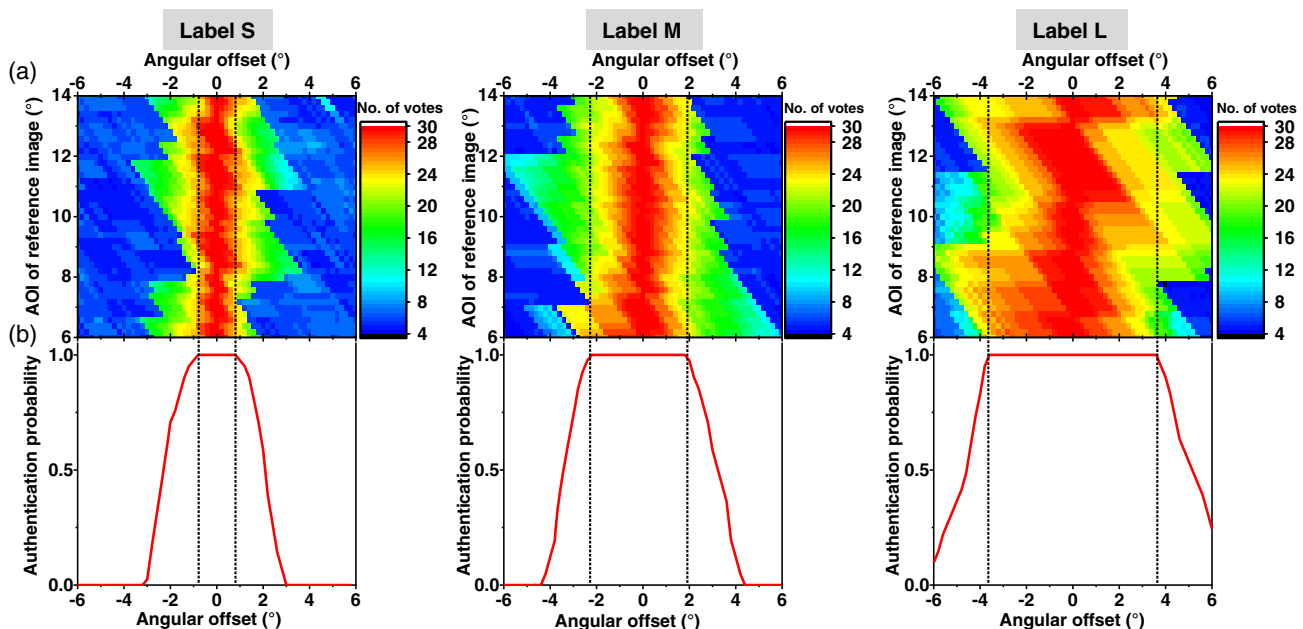


Figure 4. a) Number of votes from the authentication algorithm for test images with the noted angular offset from a reference image. To increase the number of comparisons, reference images at the various initial AOIs as indicated were used. b) Authentication probability versus AOI angular offset between the reference and test images (based on a threshold of 16 votes) for different labels. The dotted lines show the AOI tolerance, the maximum offset in AOI between reference and test images for which probability of authentication is greater than 0.99.

we robustly define the AOI tolerance as the maximum angular offset from the reference image for which a test image has an authentication probability higher than 99%. The data in Figure 4b show this to be a good definition for the AOI tolerance, the probability of authentication drops suddenly from essentially unity at a given angle.

Figure 5a reproduces the authentication probability curves for all labels on a single graph and Figure 5b presents the dependence on the AOI tolerance on the particle size. The AOI tolerance increases from 0.8° to 2.0° and finally to 3.6° as the particle size increases. The relationship between particle size and AOI tolerance appears roughly linear over the range of particles and AOIs investigated. The linear relationship between AOI tolerance and particle size is expected if: 1) the particles are large enough that the diameter of the illumination focal spot is small compared to the particle diameter; and 2) the particles are small enough that the approximation that $\sec^2\theta \approx 1$ is valid at the AOI at which the focal spot no longer is in the particle. Considering wave optics, we can estimate that the diameter of the focal spot is around 1.6 μm for this design (see Supporting Information, Section 5). The diameter of our smallest particles (9 μm) is almost an order of magnitude greater than the focal diameter, thus the approximation that the excitation light can be considered as an infinitely small point is just beginning to become valid. Moving to smaller particles, the AOI tolerance would eventually not continue to decrease linearly with particle size (as the size of the excitation radius would need to be considered). To consider the largest particle size for which the linear dependence of AOI tolerance on particle size remains valid, we note that the deviation caused by $\sec^2\theta \approx 1$ reaches 10% at 18°. In this design, the lateral shift of the focus is 180 μm at 18°, so particles at least up to diameters of 180 μm should continue with the linear trend of AOI tolerance on particle size.

Our results demonstrate that moving to shorter focal length microlenses and control of the microparticle phosphor size allows the tolerance of our labels to AOI mismatch between the reference and test images to be controlled. As the AOI tolerance increases, a test image taken with a larger angular offset from the reference image will still result in a positive authentication. The probability of a false authentication between different

labels is not affected. The implications for practical implementation of this label technology and further directions for development will be briefly discussed now.

3. Discussion

For practical implementation of anticounterfeiting labels based on a MLA laminated to a microphosphor-doped layer, it is favorable that there is a greater tolerance of the bright point pattern to the AOI. If test and reference images with greater difference in the AOI still authenticate, i.e., the AOI tolerance is increased, then less precise control of the label relative to the excitation source is needed in field authentication equipment. This is favorable in terms of reducing system cost, and expanding the number of possible use-cases.

To make the discussion of the impact of AOI tolerance on authentication hardware more concrete, we consider an example use-case of this technology in the authentication of medication in blister packs. A schematic of a simple apparatus into which the blister pack is inserted is shown in Figure 6. Guides, illustrated in brown, control the angle and depth of insertion of the blister pack along a bed, shown in white, that holds the package 10 cm from a row of 3 LEDs. The LEDs are spaced and angled to illuminate the label in a transparent portion of the blister pack (where an aluminum lid foil is not applied) at -10° , 0° , or 10° AOIs. The LEDs are turned on one at a time, and an image of the bright point pattern is captured for each AOI by the camera unit (black box with orange stripes) on the top side of the apparatus. Different bright point-patterns are then sent to be checked against the database by an onboard computer. Such a system could be easily modified to authenticate other products with transparent plastic packaging, such as blister-packed medications. The best AOI tolerance we achieve here, 3.6°, corresponds to a lateral shift of 6 mm between the labeled package and the LED strip. Controlling the placement to this tolerance by using simple mechanical guides as shown should be possible.

Returning to methods to physically redesign the labels for further improvement in the AOI tolerance, it should be possible to reduce the focal length of microlenses even further by laminating or embossing them directly onto or into the microparticle-

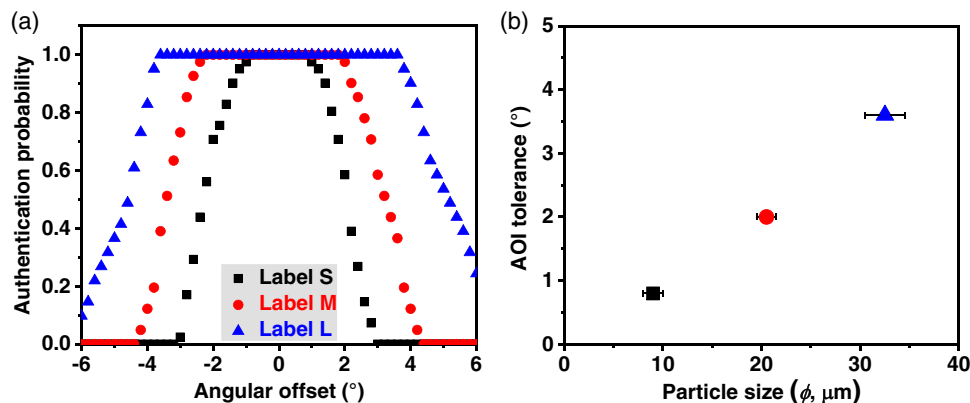


Figure 5. a) Authentication probability as function of angular offset between the reference and test images for labels using various particle sizes. b) Tolerance for change in AOI less than which the authentication probability remains greater than 0.99 as a function of the D50 particle size in the labels.

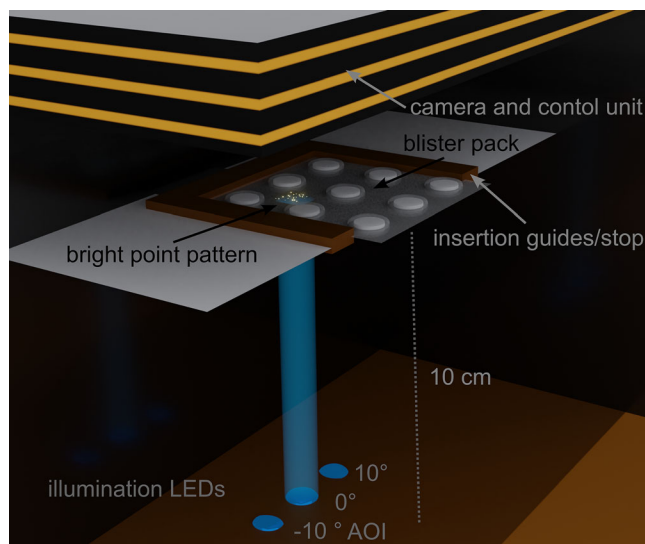


Figure 6. Illustration of potential application of the unclonable labels in blister packed medication. The microlens array could be located on one side of a 400 μm -thick polymer substrate. The aluminum lidding seal is removed from a patch on the other side. This would allow authentication in the simple apparatus shown, where three fixed LEDs could provide illumination at -10° , 0° , and 10° AOI. The 3.6° angular tolerance would require a deviation of less than 6 mm in the positioning of the label when the LEDs are 10 cm distant.

containing layer (currently the 400 μm thick glass substrate on which the microlenses are created limits the focal length, but this constraint is removed if they are created directly on the PDMS layer). We estimate that a decrease in the focal length and a corresponding increase in the AOI tolerance of roughly a factor of 2 should be possible with this approach. This would also be a step towards being able to implement this technology in polymer banknotes, whose substrate thickness much thinner than blister packs (and increasing the thickness of a polymer banknote with a security feature is unacceptable due to requirements for stacking, e.g., in automatic currency handling machines). Whereas the typical thickness of the plastic substrate for blister packs is around 400 μm , polymer banknotes are typically less than 100 μm thick—demonstrations of this technology on such thin substrates will require further work. Also, this direct embossing of the microlens array into the phosphor layer could improve the stability of the labels. The label stability (i.e., length of time over which authentication is possible) must be developed to be compatible with a several-year product shelf life. The stability of the phosphor particles themselves is not a problem in this respect, as durable microphosphors already used for example in commercial white-light LEDs are available.^[10] The stability of the microlens arrays against scratching and soiling must be carefully considered, but commercial implementations of microlens arrays on banknotes for security feature exist.^[11] Thus, an overall stability on the order of years should be possible with this design. However, when retesting one of our prototype labels 1 year after fabrication we note that authentication is not reliable (see Supporting Information section 6). Although a detailed analysis of stability will be considered in future work, we hypothesize that

slight shifting of the glass substrate relative to the microphosphor doped layer could occur in the current design. This would lead to a shift of the MLA with respect to the random phosphor particle distribution, and thereby compromise label stability. This would be alleviated with direct lamination of the microlenses into the doped polymer layer.

4. Conclusion

This study reports the fabrication of a series of unique, unclonable labels for anti-counterfeiting based on a MLA and commercial DS phosphors with varying D50 diameters on the micron scale. The AOI tolerance, the maximum difference in AOI between a reference and test image for which the test image still authenticates, increases with the D50 particle diameter. For D50 particle diameters of 9.0 ± 1 , 20.5 ± 1 , and 32.5 ± 2 μm , the AOI tolerances were 0.8° , 2.0° , and 3.6° , respectively. This represents a nearly twenty-fold increase in the tolerance compared to our original design that employed longer focal length microlenses and self-synthesized UC particles of size on the order of 10 μm . At the current level of development, we suggest that this label technology could be applied to mark blister packs, where the transparent polymer substrate provides an ideal foundation for applying a microlens array to one side and the particle doped layer to the other. Further development of the technology to allow application on thinner substrates may open possibilities for currency authentication. Ultimately, it would be extremely attractive if a single smartphone could be used to authenticate the label (providing excitation via its flashlight and capturing the bright point patterns using its camera). The understanding of the AOI tolerance gained herein will be of use in guiding future designs towards this goal.

5. Materials and Methods

Details for the Preparation of Labels: The silicone elastomer (SYLGARD 184, Dowsil, RTV-615, Component-A) was taken as the base component. The DS phosphors (YYG isiphor, Sigma-Aldrich, 0.5 wt%) were uniformly dispersed in the RTV-A elastomer using a high-speed dispersion device (CAT M. zipper GmbH, 6–8 min). Thereafter, the mixture was kept under vacuum for 10 min at room temperature to remove the incorporated air bubbles and lower its temperature. Following this, RTV component-B, which was a cross-linking additive to RTV-A, was added to the solution and mixed manually using a flat spatula for 2–3 min. The mass ratio of the RTV components A and B in the final solution was 10:1. The resulting solution was reprocessed under vacuum for 12–15 min. Finally, the solution was poured on a 1 mm-thick glass substrate with spacers of height 200 μm . As shown in Figure 2a, the phosphor-doped PDMS solution was covered from the top using a 400 μm thick glass substrate and cured on a hot plate at 120°C for 15–20 min.

The microlens array (MLA) was designed in the Matlab program and printed on a 1 mm ITO-coated glass substrate using a two-photon lithography technique on IP-S (Nanoscribe) photoresist. Since the refractive index of glass material and IP-S was the same in the visible wavelength, the use of an ITO-coated glass substrate was required for refractive index mismatching. This helped the lithography machine to easily find the interface position to start the printing. Two hundred fifty-six microlenses (16×16) were developed in a square packing manner without any inter-lens spacing.

For multiple-replication of the MLA structure on a glass substrate, a master substrate was prepared by first depositing an aluminum oxide

(Al₂O₃) layer (≈30–50 nm thick) on the printed MLA substrate using the pulse-laser deposition (PLD) technique. Following the plasma-etching of the metal oxide-coated MLA substrate, it was treated with an antiadhesive solution under vacuum. The antiadhesive solution contained a 20 millimolar concentration of PFOTS silane (trichloro-1H, 1H, 2H, 2H-perfluorooctyl-silane, Sigma-Aldrich) in cyclohexane solvent, which attached to the plasma-etched Al₂O₃ surface of the MLA master substrate. Thereafter, a 10:1 mass ratio of RTV components A and B were used to fabricate an inverse structure of MLA from the silane-coated MLA master texture under vacuum, wherein the RTV solution was poured on the MLA master texture bounded by a 5 mm-thick brass mold. The inverse structure of MLA developed on PDMS was further coated by the antiadhesive layer in the desiccator (under vacuum), following the same procedure as mentioned above. Now, the NOA-88 (Norland optical adhesive) photoresist was dropped on a 400 μm-thick glass substrate and covered by the MLA inverse-structured PDMS matrix (Step 4, Figure 2a). The entire system was placed under vacuum for 15 min to eliminate air bubbles from the NOA material, trapped in between the negative MLA PDMS and the glass substrate (Step 5, Figure 2a). Following the vacuum step, the sample was treated with UV light which cured the NOA photoresist. After the UV treatment, the inverse-structured PDMS was detached from the MLA replicated glass substrate (Step 6, Figure 2a). Herein, the coating of the antiadhesive layer on the inverted MLA surface of PDMS helped in easy separation of the NOA cured MLA from the cured PDMS matrix.

Experimental: Three labels (S, M, and L), each doped with different-sized DS particles, but similar MLA were prepared. For analysis, the labels were mounted on a 3D-printed sample holder, which was fixed on a motorized rotation stage (CR1/M-Z7, Thorlabs). The motion of the rotation stage was controlled by a Kinesis K-cube brushed DC servo motor controller (KDC 101, Thorlabs). A 450 nm LED (M450LP1, Thorlabs), placed at a distance of 10 cm from the front surface of the label was used for illumination. A full-high-definition (FHD) scientific CMOS camera (CS2100M, Thorlabs), fitted with an 18–108 mm zoom lens (MVL7000, Thorlabs) was used to a focal length of 108 mm to capture the luminescent point-pattern image from the labels. The camera was slightly off-axis at ($\theta_{\text{cam}} = 10^\circ$) to the LED illumination and was focused on the back surface of the label. The camera was kept at 32 cm from the label and a 500 nm long-pass filter (FEL0500, Thorlabs) was inserted before the camera aperture to filter out the excitation beam. The exposure time of the camera to capture each image was set to 2 s. A three-second wait time was included in the camera operation for capturing the next AOI image following the stage rotation. 100 images were recorded from AOI = 0° to AOI = 20°, with a 0.2° step. For each label, the 100 luminescent images were recorded and saved in a total of 500 s (about 8 and a half minutes). A technical schematic illustrating the label's unclonability concept to the real-world application was provided in the Supporting Information, Section 7.

Pattern Authentication Algorithm: This section briefly explains the algorithm used to authenticate a label via verifying two luminescent point-pattern images captured from the labels.

- I. The grayscale image is binarized into a (1080 × 1920) matrix array form, and continuous regions of “1” are determined in each binary image.
- II. The center position of each continuous region is sorted into a list as points $P(p_x, p_y)$. Further, we truncate the list to N points.
- III. A list of points, $P(p_x, p_y)$ is generated for a reference image, and a list of points $Q(q_x, q_y)$ is generated for the test image.
- IV. To make a comparison between a reference and a test image, we select the first x basis-points in each image which can be chosen as basis-pair.
- V. For each basis pair, we find a transformation matrix ($T(i, j, k, l)$) for mapping $(q_k, q_l) \rightarrow (p_i, p_j)$. We use this transformation matrix ‘ T ’ for finding the $\frac{(x^2 - x)}{2}$ transformed lists $Q'(i, j, k, l) = QT(i, j, k, l)$.
- VI. A comparison of points P and all Q' is made, which results in a number called “vote.” A vote is cast for every point in all Q' within a threshold distance “ d ” to a point in P . We remove the multiple vote cast for the same point in P (for excluding the basis pair matches).

VII. The Q' with the highest number of votes is considered the best match.

VIII. To select a threshold vote for the authentication decision, we put a label on the sample stage, capture the luminescence point pattern images at known AOIs, and save it as ‘Reference’ images. Now, we take out the label from the sample stage, reposition it back, and capture the point pattern at the same AOIs as before. We do the same procedure of measurement with a second label.

A one-to-one comparison of all test images with the reference images is made. The comparison gives the distribution of votes for the same images and different images. The vote number for “same images” originates from the same label and same AOI. Whereas vote number for “different images” originates from the different label, or it can be from the same labels but at different AOIs.

Supporting Information

Supporting Information is available from the Wiley Online Library or from the author.

Acknowledgements

The authors gratefully acknowledge the Helmholtz Association for funding through : 1) a Recruitment Initiative fellowship for B.S.R.; 2) the Helmholtz Materials Energy Foundry (HEMF); 3) Karlsruhe Nano Micro Facility for Information driven Material Structuring and Characterization (KNMFi) to providing the microfabrication facility; and 4) Research Field Energy – Program Materials and Technologies for the Energy Transition- Topic 1 Photovoltaics. The author V.K. acknowledges DAAD for financial support. The authors thank Dr. Dirk Fuchs at the Institute for Quantum Materials and Technologies, KIT for providing the facility of the pulsed laser deposition (PLD) of the metal oxide (Al₂O₃) nano-layer on the MLA substrate.

Open Access funding enabled and organized by Projekt DEAL.

[Correction added on June 3, 2022, after first online publication: Projekt DEAL funding statement has been added.]

Conflict of Interest

A patent application has been filed by the authors related to the work presented in this manuscript.

Data Availability Statement

The data that support the findings of this study are available from the corresponding author upon reasonable request.

Keywords

anticoounterfeiting, microlens arrays, unclonable labels

Received: July 13, 2021

Revised: November 4, 2021

Published online: January 6, 2022

- [1] a) M. K. P. Stryzowski, S. Jacobzone, N. Wajzman, *Trends in Trade in Counterfeit and Pirated Goods*, OECD Publishing (OECD/EUIPO), Paris, 2019; b) U. B. J. Hardy, L. Bonnier, S. Betti, S. Padmanaabhan, C. Braddon, *Mapping the Impact of Illicit Trade on the Sustainable Development Goals*, Transnational Alliance To Combat Illicit Trade (TRACIT), 2019; c) P. Aldhous, *Nature* 2005,

- 434, 132; d) J. Spink, D. L. Ortega, C. Chen, F. Wu, *Trends Food Sci. Technol.* **2017**, *62*, 215.
- [2] Frontier Economics, *The Economic Costs of Counterfeiting and Piracy*, Report 40 prepared for BASCAP and INTA, Frontier Economics Ltd, Brussels, Belgium, Vol. 2, **2017**, p. 26 <https://jicwbo.org/publication/economic-impacts-counterfeiting-piracy-report-prepared-bascap-inta/>.
- [3] a) N. Torun, I. Torun, M. Sakir, M. Kalay, M. S. Onses, *ACS Appl. Mater. Interfaces* **2021**, *13*, 11247; b) A. Alharbi, D. Armstrong, S. Alharbi, D. Shahrjerdi, *ACS Nano* **2017**, *11*, 12772; c) Z. Hu, J. M. M. L. Comeras, H. Park, J. Tang, A. Afzali, G. S. Tulevski, J. B. Hannon, M. Liehr, S.-J. Han, *Nat. Nanotechnol.* **2016**, *11*, 559; d) J. W. Leem, M. S. Kim, S. H. Choi, S.-R. Kim, S.-W. Kim, Y. M. Song, R. J. Young, Y. L. Kim, *Nat. Comm.* **2020**, *11*, 1; e) R. Pappu, B. Recht, J. Taylor, N. Gershenfeld, *Science* **2002**, *297*, 2026; f) L. Tian, K.-K. Liu, M. Fei, S. Tadepalli, S. Cao, J. A. Geldmeier, V. V. Tsukruk, S. Singamaneni, *ACS Appl. Mater. Interfaces* **2016**, *8*, 4031; g) R. Arppe, T. J. Sørensen, *Nature Reviews Chemistry* **2017**, *1*, 0031.
- [4] P. Kumar, K. Nagpal, B. K. Gupta, *ACS Appl. Mater. Interfaces* **2017**, *9*, 14301.
- [5] M. Xie, F. Xu, L. Zhang, J. Yin, X. Jiang, *ACS Macro Lett.* **2018**, *7*, 540.
- [6] T. Ma, T. Li, L. Zhou, X. Ma, J. Yin, X. Jiang, *Nat. Comm.* **2020**, *11*, 1811.
- [7] K. Park, K. Jung, S. J. Kwon, H. S. Jang, D. Byun, I. K. Han, H. Ko, *Adv. Funct. Mater.* **2016**, *26*, 7836.
- [8] R. Arppe-Tabbara, M. Tabbara, T. J. Sørensen, *ACS Appl. Mater. Interfaces* **2019**, *11*, 6475.
- [9] V. Kumar, Dottermusch, S., Katumo, N., Richards, B. S., Howard, I. A. (Preprint), arXiv: 2107.05439, unpublished, May **2021**.
- [10] a) C. C. Lin, R.-S. Liu, *J. Phys. Chem. Lett.* **2011**, *2*, 1268; b) Y. Yang, F. Wu, H. Yu, Y. Hu, C. Qiu, J. Li, H. Zhang, X. Wang, L. Wei, B. Liu, *Optik* **2020**, *200*, 163455.
- [11] *Crane currency- The global banknote expert*, <https://www.cranecurrency.com/products-services/motion/> (accessed: November 2021).